Page Proof Instructions and Queries

Thank you for choosing to publish with us. This is your final opportunity to ensure your article will be accurate at publication. Please review your proof carefully and respond to the queries using the circled tools in the image below, which are available in Adobe Reader DC* by clicking **Tools** from the top menu, then clicking **Comment.**

Please use *only* the tools circled in the image, as edits via other tools/methods can be lost during file conversion. For comments, questions, or formatting requests, please use $\boxed{\text{T}}$. Please do *not* use comment bubbles/sticky notes $\bigcirc$.

| Comment ▾ | $\bigcirc$ | $\oslash$ | T̲ | $\ominus$ | $\ominus$ | $T_\wedge$ | T | $\boxed{\text{T}}$ | $\oslash$ | ✐ | 🖈▾ | 📎▾ | ✑▾ |
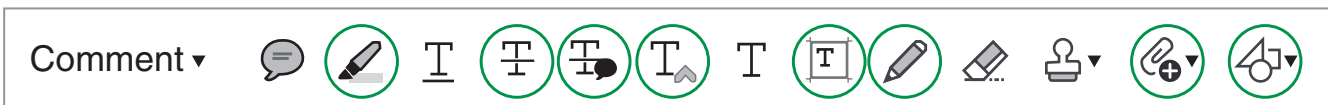
*If you do not see these tools, please ensure you have opened this file with Adobe Reader DC, available for free at get.adobe.com/reader or by going to Help > Check for Updates within other versions of Reader. For more detailed instructions, please see us.sagepub.com/ReaderXProofs.

No.	Query
	Please note that we cannot add/amend ORCID iDs for any article at the proof stage. Following ORCID's guidelines, the publisher can include only ORCID iDs that the authors have specifically validated for each manuscript prior to official acceptance for publication.
	Please confirm that all author information, including names, affiliations, sequence, and contact details, is correct.
	Please review the entire document for typographical errors, mathematical errors, and any other necessary corrections; check headings, tables, and figures.
	Please confirm that the Funding and Conflict of Interest statements are accurate.
	Please ensure that you have obtained and enclosed all necessary permissions for the reproduction of artistic works, (e.g. illustrations, photographs, charts, maps, other visual material, etc.) not owned by yourself. Please refer to your publishing agreement for further information.
	Please note that this proof represents your final opportunity to review your article prior to publication, so please do send all of your changes now.
AQ: 1	Please provide the volume number in ref. 5.
AQ: 2	Please provide the volume number and page range in ref. 10.
AQ: 3	Please provide the page range in ref. 11.
AQ: 4	Please provide complete details in ref. 20.
AQ: 5	Please provide the volume number in ref. 37.
AQ: 6	Please provide complete details in ref. 38.
AQ: 7	Please provide the volume number in ref. 43.
AQ: 8	Please provide the volume number and page range in ref. 54.

A comparison between rotating squares and anti-tetrachiral systems: Influence of ligaments on the multi-axial mechanical response

Luke Mizzi, Andrea Sorrentino, Andrea Spaggiari [iD] **and Davide Castagnetti** [iD]

Abstract
Rotating unit systems are one of the most important and well-known classes of auxetic mechanical metamaterials. As their name implies, when loaded, these systems deform primarily *via* rotation of blocks of material, which may be connected together either directly through joints (or 'joint-like' connections made by overlapping vertices of the rotating units) as in the case of rotating rigid polygonal-unit systems or by ligaments/ribs as in the case of chiral honeycombs. In this work, we used Finite Element Analysis to investigate the effect which the presence/absence of ligaments has on the on-axis and off-axis mechanical properties of these systems by analysing two of the most well-known structures which characterise these two cases: the rotating square system and the anti-tetrachiral honeycomb. It was found that while the presence of ligaments has a negligible effect on the on-axis Poisson's ratio of these systems, it has a profound influence on nearly all other mechanical properties as well as on the off-axis loading behaviour. Systems with ligaments were found to exhibit a high level of anisotropy and also a severely reduced level of stiffness in comparison to their non-ligamented counterparts. On the other hand, the rotating square system suffers from high localized stress-intensities and has a very low strain-tolerance threshold. In addition, an optimized 'hybrid' geometry which is specifically designed to capture the best features of both the anti-tetrachiral and rotating square system, was also analysed. This work shows the main differences between ligament-based and non-ligament-based auxetic structures and also highlights the importance of considering the off-axis mechanical response in addition to the on-axis properties when investigating such systems.

Keywords
Auxetics, mechanical metamaterials, rotating squares, chiral honeycombs, Poisson's ratio

Date received: 3 June 2021; accepted: 9 August 2021

Introduction

Auxetics are systems or materials which possess the unusual property of a negative Poisson's ratio.[1,2] This means that these systems expand in the transverse direction when subjected to a uniaxial tensile load. This property arises primarily from the geometry and deformation mechanisms of the systems and, as a result of this, auxeticity is considered to be scale-independent. Therefore, should any geometry or mechanism which imparts auxetic behaviour at the macroscale be replicated at the micro- and nanoscale, it is expected to function in virtually the same manner. Auxetic systems also exhibit a variety of other anomalous characteristics including synclastic curvature,[3] high indentation resistance,[4,5] high shear resistance[6,7] and energy absorption,[8,9] which makes them suitable for niche applications such as stents,[10] deployable antennas,[11] flexible electronics[12] and prosthetics.[13]

There are various geometries which give rise to auxeticity, with the most well-known being re-entrant structures, including hexagonal honeycombs and star-shaped geometries,[14–17] rotating unit systems,[18–20] chiral honeycombs,[21–27] buckling-based architectures[28,29] and folding/origami metamaterials.[30]

Department of Engineering Sciences and Methods, University of Modena and Reggio Emilia, Reggio Emilia, Italy

Corresponding author:
Luke Mizzi, Department of Engineering Sciences and Methods, University of Modena and Reggio Emilia, Reggio Emilia, Italy.
Email: luke.mizzi@unimore.it

These systems, both 2 D and 3 D, have the potential to exhibit a near-infinite range of negative Poisson's ratios as well as other mechanical properties *via* a number of diverse deformation mechanisms. This design versatility is extremely advantageous to the engineer/researcher implementing these systems in real-life applications since, in theory, it allows one to pick and choose the metamaterial geometry which matches the desired design specifications. However, in order for this to become a reality, a complete library containing all the relevant knowledge required for the implementation of these auxetic systems is required. Besides on-axis Poisson's ratios and Young's moduli (the most oft-studied and commonly evaluated properties), other important characteristics such as off-axis mechanical properties, performance under high strain conditions (including strain tolerance limits, fracture and fatigue strength), influence of material properties and density spectrum need to be studied. Despite the large number of studies on auxetic metamaterials found in the literature, further research is required in order to fill in the gaps in the state-of-the-art for a number of geometries, which limits their usefulness at the moment.

Two of the most well-known auxetic systems which are found in literature are the rotating squares[18] and anti-tetrachiral[23,31] honeycombs (shown in Figure 1). Both these systems, in their regular and ideal states, exhibit a Poisson's ratio of *ca.* −1 and share a number of geometric features including two axes of mirror symmetry and a square unit cell. Moreover, if one considers the anti-tetrachiral variant shown in Figure 1, which has a square-shaped chiral node instead of the traditional circular one, the only geometric difference between the two systems is the presence of ligaments connecting the square units in the latter and their absence in the former.[32] Both these systems also deform in a very similar manner when uniaxial loaded in an on-axis direction; through rotation of

the square blocks of materials, which is accompanied by flexure of the ligaments in the anti-tetrachiral honeycomb. These two systems have been extensively studied throughout the years using analytical, numerical and experimental techniques.[18,23,31,33–35] They have also been investigated in various related forms, apart from the ideal and regular geometries shown in Figure 1, including as perforated systems,[36–43] non-porous structures,[44] composites,[45,46] sandwich systems[47,48] and even irregular variants.[49–52]

The majority of these studies have focused mainly on the on-axis properties of these two geometries and it has been well established that, while both have an identical Poisson's ratio, the main difference between them is that the rotating square system is much stiffer than its anti-tetrachiral counterpart, while the latter system has a much better stress distribution throughout the system upon the application of a specific strain, leading to improved strain tolerance and affording greater deformability. However, studies focusing on the off-axis properties as well as the shear modulus of these two structures are few and far in between. It is imperative that these characteristics are also properly understood, since they are key to determining the mechanical response in cases involving the implementation of such metamaterials in applications where they may be subjected to off-axis or non-uniform loading conditions such as blast loading and impact conditions[8,53] and are also required for the determination of the compliance matrix of anisotropic systems. Therefore, in this work, we aim to investigate the similarities and differences in the responses of these two sets of geometrically-related mechanical metamaterials to on-axis and off-axis loading conditions. To this end, a range of systems pertaining to these two classes of geometries were constructed and simulated under on-axis and off-axis loading using Finite Element analysis. In addition, an optimized 'hybrid' geometry
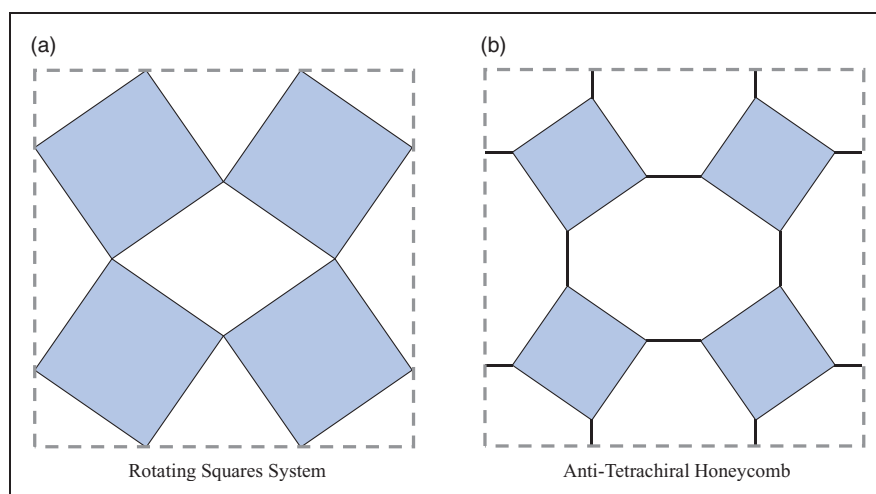

Figure 1. Diagrams showing the unit cells of a typical idealised version of (a) a rotating squares system and (b) an anti-tetrachiral honeycomb with square chiral nodes. Note that the main difference between these two systems is the presence of ligaments.

which shares features from both types of structures was also analysed in order to ascertain to what extent it is possible to capture the best mechanical characteristics of both systems.

Methodology

The structures investigated in this work were simulated using the ANSYS16 Multiphysics Finite Element software. The simulations conducted in this work may be divided into two main parts: first, a range of rotating square and anti-tetrachiral honeycombs were studied in order to evaluate the effect of ligament length on mechanical properties, and, secondly, an optimized 'hybrid' geometry was modelled and its mechanical response compared with those of two corresponding rotating squares and anti-tetrachiral honeycombs.

Simulations on rotating squares and anti-tetrachiral systems

Both the rotating squares and anti-tetrachiral systems may be defined by a common set of geometric parameters, as shown in Figure 2. The side length of the square unit was defined by the parameter a, while the angle between the rotating units was denoted by θ. The ligaments were defined by the thickness parameter, t, and their length, l (see Figure 2(a)). The rotating square system naturally corresponds to a system with $l = 0$. As shown in Figure 2(b), the two square units are connected directly to each other with an overlap distance, w. For the systems containing ligaments, the parameter w was used to define the overlap of the ligaments with the square units. This degree of overlap is necessary in order to ensure that the vertices resulting from the bridging connection of the ligaments with the square units can be filleted and as a consequence the effective ligament length is equal to roughly l–$2w$ for the systems possessing ligaments. Finally, all sharp corners within the system were filleted with a fixed radius, r.

In order to investigate the influence of the ligaments on the mechanical properties of these systems, various different geometries were constructed and analysed. Since ligament length, i.e l, is the main feature in which these two sets of systems differ, this
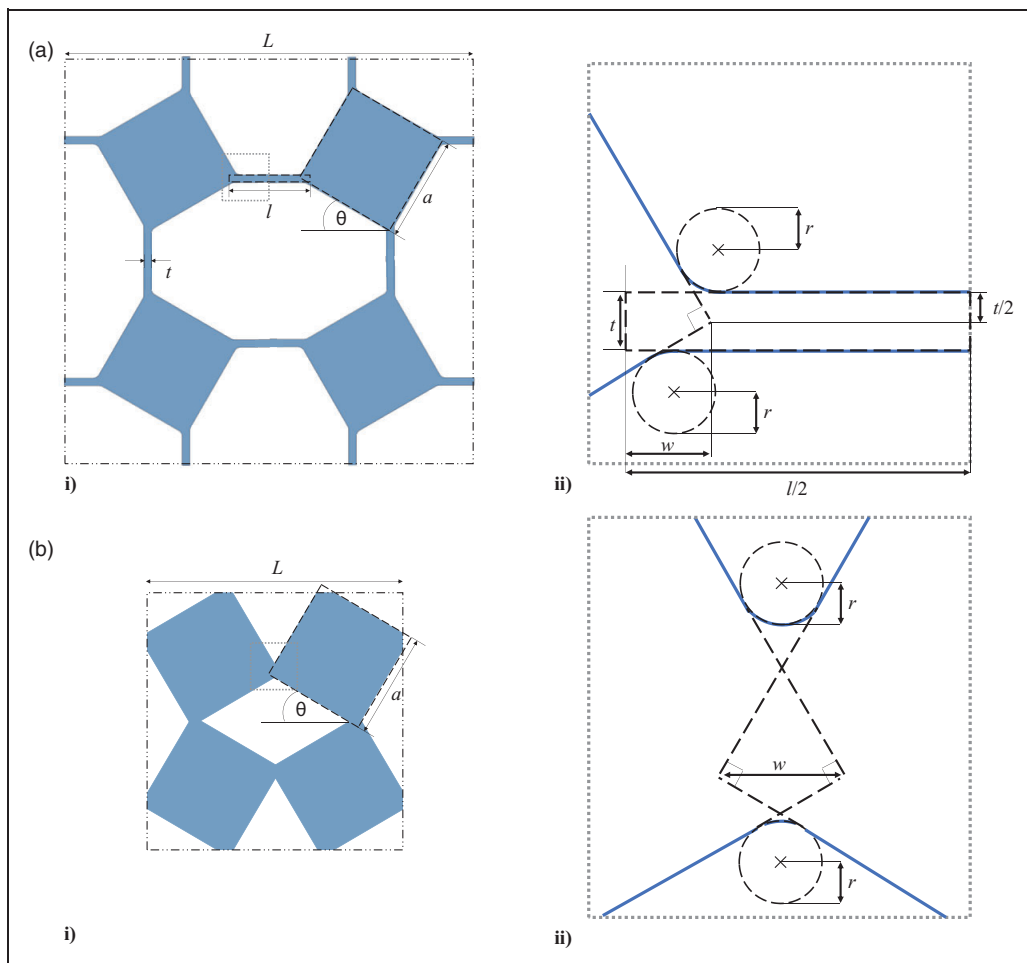

Figure 2. Diagram indicating the geometric parameters used to define the systems studied here. Figure (a) shows an anti-tetrachiral system, where all the geometric parameters are required to describe the system, while in the case of the rotating square system (b), the ligament length, l, is zero and the 'square' units are connected to each other directly with an overlap distance, w.

dimension (shown in Figure 2) was the main parameter varied according to the following values: 0, 2, 4, 8, 16 mm. The parameters w, r and t were kept constant at all times at values of 0.3, 0.1 and 0.3 mm respectively. The parameter θ was also fixed at a single value; 30°, which results in a system which is close to neither being fully-opened nor fully-closed. The full list of parameters is presented in Table 1. Using these geometric parameters, two sets of structures were simulated. The first set involved structures where the parameter a was kept constant at a value of 20 mm at all times, resulting in 'square' block of material remaining the same size and the overall size of the representative unit cell increasing as the ligament length, l, increases. For the second set, the overall representative unit cell length, L, was kept constant at a value of 118 mm at all times, with the parameter a decreasing as the ligament length increases. For both these sets, the systems with a ligament length of 32 mm are almost identical. These conditions were set in order to allow for consideration of the influence of ligament length with respect to both rotating unit size and overall representative unit cell of the entire system since these parameters are related as follows:

$$L = 2a(\sin\theta + \cos\theta) + 2(l - 2w) \tag{1}$$

$$a = \frac{L - 2(l - 2w)}{2(\sin\theta + \cos\theta)} \tag{2}$$

The systems were simulated as a single unit cell under periodic boundary conditions with a plane-stress model. The PLANE183 element was used (quadratic higher order 2 D 8-noded element with two translational degrees of freedom at each node and quadratic displacement behaviour), with a minimum mesh size of $t/3$. The final element size was chosen following a mesh convergence study conducted on

two extreme systems – one with no ligaments and the other with long ligaments ($t = 32$ mm) – the results of which are presented in Figure 3(c). The linear material properties of isotropic structural steel were used: $E_{mat} = 200$ GPa and $\nu_{mat} = 0.3$. Since two different orientations were studied, i.e. the typical on-axis form and the rotated one at 45°; the minimum representative unit cells used are distinctly different, with the former being made up of four rotating units and the latter two (see Figure 3(a)). Periodicity was induced through the use of constraint equations which control the displacement of nodes on opposing edges in the x and y-directions. These constraint equations, shown in equations (3) and (4), were applied on all edge nodes as follows. First, the meshes on opposing edges were mapped in order to ensure that they are identical. Then, a pair of master nodes (one on the right and another on the left edge) are chosen and the total displacements in the x- and y-directions of these nodes is bound to that of all other pairs of (slave) nodes using equations (3) and (4), where $U_{x,M1}$ denotes the x-displacement of the master node on Edge 1, $U_{x,M2}$, the x-displacement of the master node on the opposing edge (Edge 2) and $U_{x,S1}$ and $U_{x,S2}$, the same corresponding displacement for the pair of slave nodes. The same relationships are also applied for the y-displacements.

$$U_{x,M1} - U_{x,M2} - U_{x,S1} + U_{x,S2} = 0 \tag{3}$$

$$U_{y,M1} - U_{y,M2} - U_{y,S1} + U_{y,S2} = 0 \tag{4}$$

Following the implementation of the constraint equations on all edge nodes, the system was fixed in space from one node on the bottom edge of the unit cell and from a corresponding point on the opposite edge in order to constrain the system to remain aligned along the y-axis at all times during

Table 1. Complete list of geometric parameters and loading conditions for the first set of structures modelled and simulated.

| Geometric parameters						
Constant dimensions						
Overlap parameter, w				0.3 mm		
Fillet radius, r				0.1 mm		
Ligament thickness, t				0.3 mm		
Pore angle, θ				30°		
Square side length, $a = 20$ mm						
Ligament length, l (mm)	0	2	4	8	16	32
Cell dimension, L (mm)	53.44	57.44	61.44	69.44	85.44	117.44
Cell dimension, $L = 118$mm						
Ligament length, l (mm)	0	2	4	8	16	32
Square side length, a (mm)	43.63	42.17	40.70	37.77	31.92	20.20
Loading conditions						
Orientations of each system simulated		0° (On-Axis), 45° (off-axis)				
Loading type		a) Uniaxial in x-direction				
		b) Uniaxial in y-direction				
		c) Simple shear in xy-plane				
Mechanical properties obtained		ν_{xy}, ν_{yx}, E_x, E_y, G_{xy}				
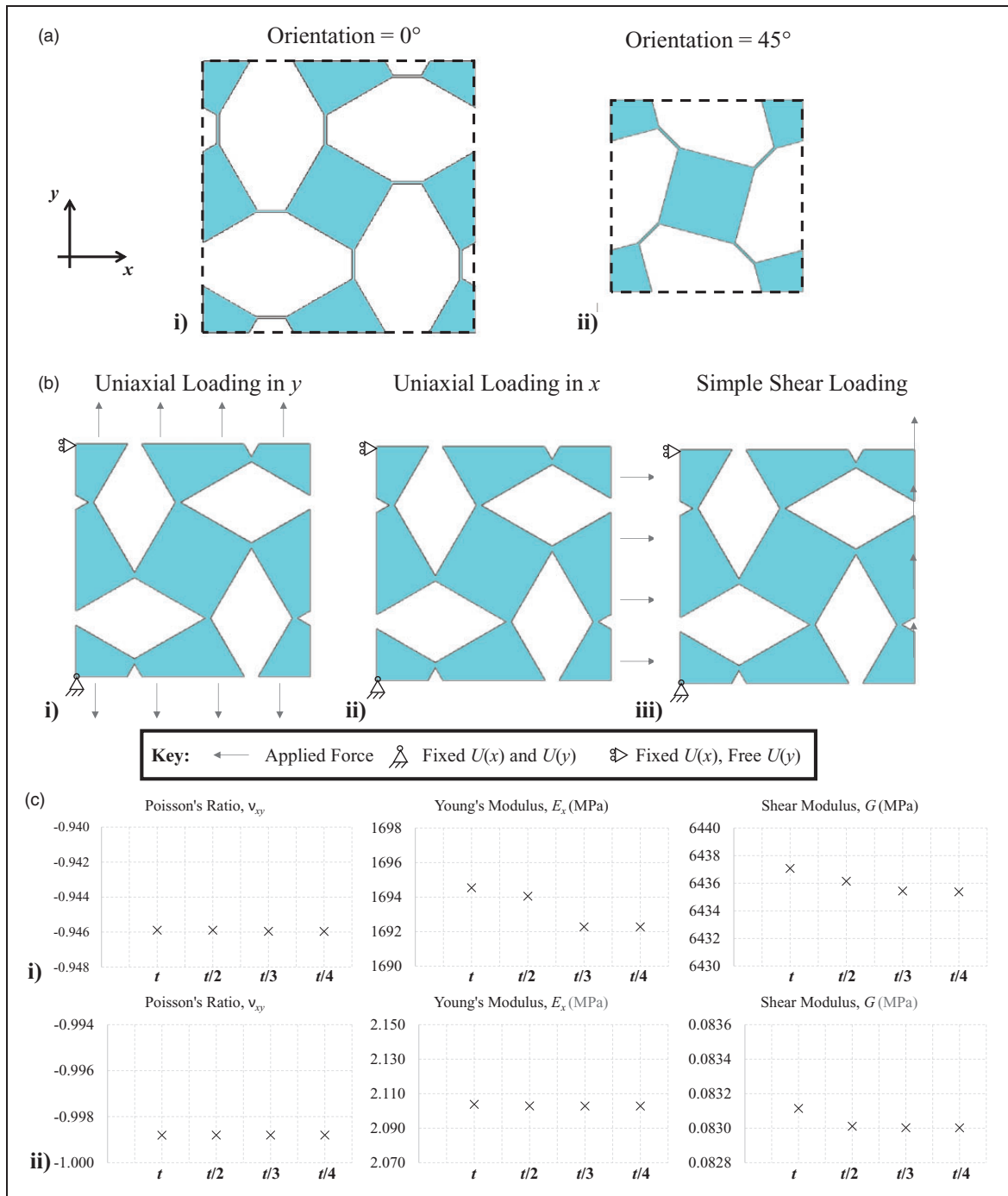
Figure 3. (a) A representative unit cell of the system (to scale) at an orientation of (i) 0° (the most commonly studied and well-known orientation) and ii) 45°. Note that while in (i) the unit cell contains four rotating units, in (ii) it contains two. In (b) the three types of loads applied to each system are demonstrated along with the fixes applied to the system to retain its alignment with the y-axis. The forces (marked in red arrows) were applied on all nodes on the edge of the unit cell and, in addition to these fixes, all edge nodes were paired to their corresponding counterparts on the opposing edge using displacement constraint equations (see Mizzi et al.[54] for more details). (c) Mechanical properties obtained for two systems, (i) $a = 20$ mm, $L = 53.44$ mm, $l = 0$ mm and (ii) $a = 20$ mm, $L = 117.44$ mm, $l = 32$ mm, using a mesh size of t, $t/2$, $t/3$ and $t/4$. The other geometric parameters were kept constant at $w = 0.3$ mm, $r = 0.1$ mm, $t = 0.3$ mm and $\theta = 30°$. Since the results obtained were extremely similar, a minimum element size of $t/3$, i.e. 0.1 mm, was chosen.

deformation and avoid rigid body motion. A detailed description of this methodology is provided in Mizzi et al.[54] The systems were subjected to two types of loads: uniaxial and simple shear loading under linear conditions (see Figure 3(b)). For uniaxial loading in

the y-direction, a unitary tensile force in the y-direction was applied on all the nodes on the upper and lower edges of unit cell, while for loading in the x-direction, a unitary tensile force in the same direction was applied on the nodes on the right and left

edges of the system. For shear loading, a force in the
y-direction was applied on all the nodes on the right
edge of the system, while an equal force, but in the
opposite direction, was applied on all the nodes on
left edge of the system. Since the system is constrained
to remain aligned with y-axis at all times, this loading
method corresponds to simple shear loading.
Following these simulations, by measuring the dis-
placements of the edge nodes, the Young's moduli
and Poisson's ratios in the x-and y-directions, E_x,
E_y, ν_{xy}, and ν_{yx}, as well as the shear modulus, G,
may be obtained for both orientations of the same
structure (assuming unit thickness in the z-direction).

Design of optimized 'hybrid' geometry and corresponding systems

In addition to this analysis, another set of simulations
was conducted on a version of the rotating squares
system with optimized interconnecting regions recent-
ly proposed by Sorrentino et al.[55] This structure,

shown in Figure 4, may be considered as a type of
hybrid rotating square/anti-tetrachiral system since
its 'joint' regions bear geometric characteristics of
both classes of auxetic structures. This system was
generated through an optimization scheme in which
the geometric parameters of the structure were varied
in order to obtain a 3% global tensile strain at a rel-
atively low stress concentration factor whilst maxi-
mizing the Young's modulus of the system and
retaining a negative Poisson's ratio below -0.95[55]
In analogy to the other geometries simulated in this
work, this structure was built according to the
following specifications (defined in Figure 4(a)):
$a = 35.36$ mm, $w = 1.30$ mm, $\theta = 30°$, $r_a = 4$ mm and
$r_b = 1$ mm. The parameter w is determined from the
dimensions θ, r_b and s, with the latter being set to
1 mm. This structure was also investigated under the
same loading conditions for orientations of 0° and 45°
and the results obtained were compared with those of
the two equivalent rotating squares and anti-
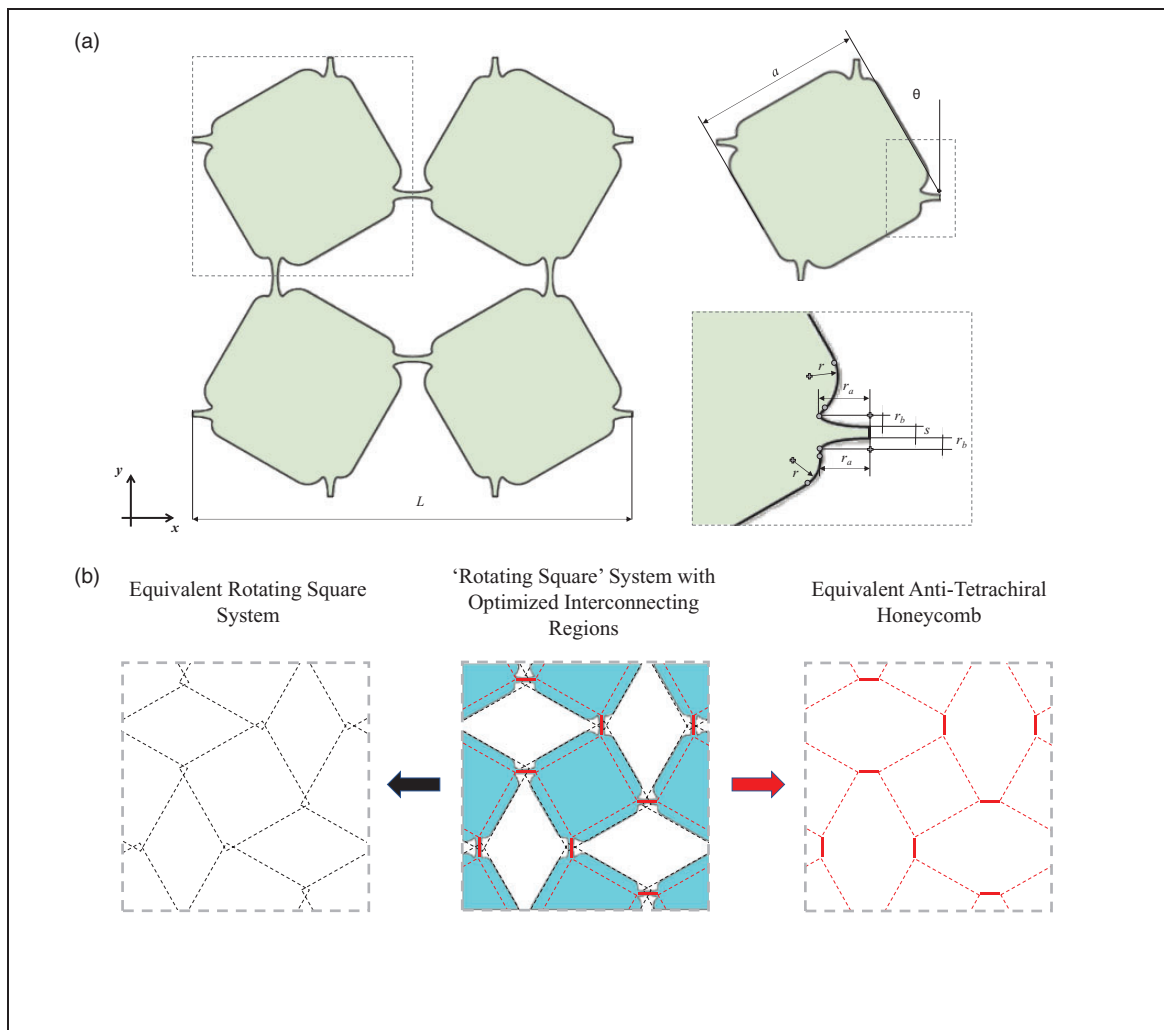tetrachiral geometries (see Figure 4(b)). The two

Figure 4. (a) A representative unit cell of the optimized rotating square geometry for improved strain tolerance and the parameters
used to defined this system. (b) Representations of the corresponding rotating square and anti-tetrachiral honeycomb systems which
bear the closest resemblance to the optimized geometry. The rotating square system has the same rotating unit size, a, as the
optimized structure, while the equivalent anti-tetrachiral honeycomb has the same ligament length, l.

equivalent structures were built, respectfully, as follows: i) $a = 35.36$ mm, $w = 1.30$ mm, $\theta = 30°$, $l = 0$ mm, $r = 0.5$ mm and ii) $a = 27.36$ mm, $w = 1.30$ mm, $\theta = 30°$, $l = 10.6$ mm, $r = 0.5$ mm, $t = 1$ mm.

Results and discussion

Rotating squares and anti-tetrachiral systems

The results obtained from the first set of simulations (based on Figure 2) are presented in Figure 5 and Table 2. In order to ensure that all of the parameters are unitless and thus the results of this study may be applied to these metamaterial geometries regardless of the base material used, the Young's moduli and shear modulus are presented as an effective percentage of the obtained modulus of the specific geometry divided by the material modulus ($E_{mat} = 200000$ MPa and $G_{mat} = 76923$ MPa) and denoted by E_x^*, E_y^* and G^*. Furthermore, in the cases of the Poisson's ratios and Young's moduli, only the results for loading in the x-direction are presented since the values obtained for loading in the y-direction were nearly identical. The mechanical properties (both Poisson's ratio and
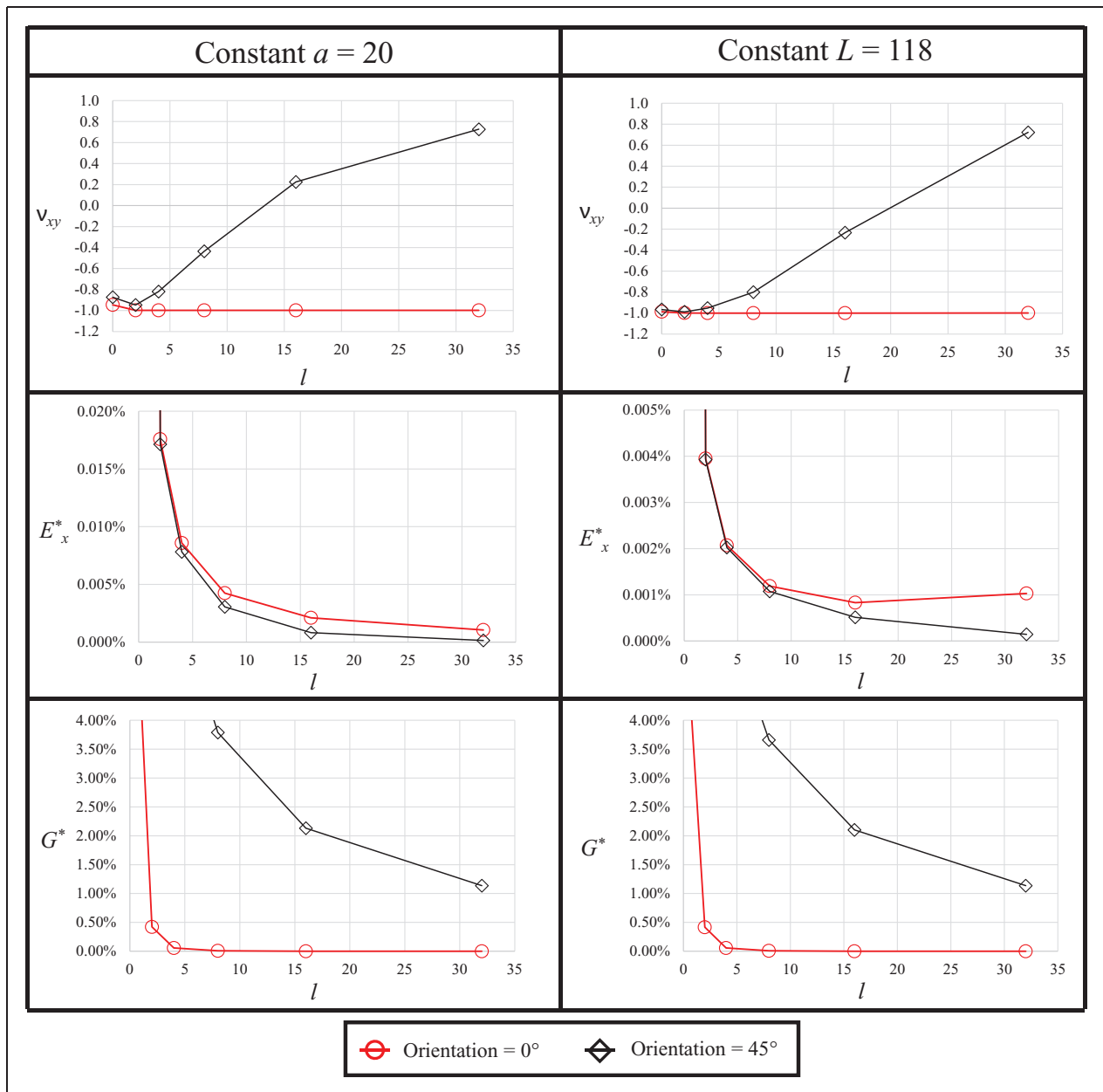

Figure 5. Plots showing the Poisson's ratios, effective Young's moduli and effective shear moduli obtained for the simulated structures with (a) constant rotating unit size and (b) constant repeating unit cell dimensions. In the cases of the Young's moduli and shear modulus, the results for systems with no or very small ligaments are not all shown on the plots due to the relatively very high value of these moduli in comparison to those observed for systems with longer ligaments, which would obscure the trends for the latter if plotted. As one can observe, the larger the ligament length, the greater the difference in mechanical properties for on-axis and off-axis loading. The full set of results are presented in Table 2 for ease of reference.

Table 2. Results obtained for each system simulated and shown in Figure 5. The other geometric parameters not listed here were kept constant as indicated in the Methodology section, at the following values: $w = 0.3$, $r = 0.1$, $t = 0.3$ and $\theta = 30°$. Note, that similar to Figure 5, the results for the Young's moduli and shear moduli are presented as effective ratios of the base material moduli ($E_{mat} = 200000$ MPa and $G_{mat} = 76923$ MPa).

l	*a*	*L*	*ν*	E^* (%)	G^* (%)
Constant *a*					
Orientation $= 0°$					
0	20	53.44	−0.9459	0.8470	8.3670
2	20	57.44	−0.9975	0.0176	0.4234
4	20	61.44	−0.9982	0.0086	0.0565
8	20	69.44	−0.9986	0.0042	0.0070
16	20	85.44	−0.9987	0.0021	0.0009
32	20	117.44	−0.9988	0.0011	0.0001
Orientation $= 45°$					
0	20	53.44	−0.8733	0.8155	20.3582
2	20	57.44	−0.9473	0.0171	9.1365
4	20	61.44	−0.8200	0.0078	6.2097
8	20	69.44	−0.4357	0.0030	3.7914
16	20	85.44	0.2244	0.0008	2.1324
32	20	117.44	0.7274	0.0001	1.1373
Constant *L*					
Orientation $= 0°$					
0	43.63	118	−0.9866	0.1705	6.3253
2	42.17	118	−0.9994	0.0040	0.4160
4	40.70	118	−0.9995	0.0021	0.0563
8	37.77	118	−0.9996	0.0012	0.0070
16	31.92	118	−0.9995	0.0008	0.0009
32	20.20	118	−0.9988	0.0010	0.0001
Orientation $= 45°$					
0	43.63	118	−0.9653	0.1687	16.5695
2	42.17	118	−0.9877	0.0039	8.3013
4	40.70	118	−0.9533	0.0020	5.8297
8	37.77	118	−0.8014	0.0011	3.6611
16	31.92	118	−0.2346	0.0005	2.1015
32	20.20	118	0.7226	0.0001	1.1372

Young's modulus) obtained for on-axis loading (Orientation $= 0°$) are congruent with those obtained from previous analytical, numerical and experimental studies on rotating square and anti-tetrachiral honeycombs.[18,23,35,36,41–43,49,50]

As one may observe from the plots in Figure 5 and the values in Table 2, there is little difference between the trends observed for the systems with a constant *a* parameter and those with a constant unit cell length, *L*. The mechanical properties of each system are, however, shown to differ significantly upon changing the orientation of the structure by 45°, with the degree of anisotropy varying extensively from structure to structure as ligament length changes. For example, in the case of the Poisson's ratio, it is clearly evident that while the Poisson's ratio remains fixed at *ca.* −1 regardless of ligament length for uniaxial loading in an on-axis direction (Orientation $= 0°$), this mechanical property varies significantly for loading in the 45° off-axis direction as ligament length increases. In fact, for the system with a ligament length of 32 mm, the Poisson's ratio becomes highly positive, with a value of 0.72, as opposed to the highly negative value of

−0.99 observed for loading in the on-axis direction. Conversely, for the systems with no ligaments (both at constant *a* and *L*), the Poisson's ratio remains negative for off-axis uniaxial loading, decreasing only slightly in magnitude. This indicates that the introduction of ligaments, and hence, the transformation of the rotating squares system to its anti-tetrachiral counterpart, despite improving the strain tolerance and deformability of this system, also comes at the cost of an increase in anisotropy and could even lead to a complete loss of auxeticity if the system is loading in an off-axis direction.

The extreme changes in Poisson's ratio for switching from on-axis to off-axis loading in the case of the anti-tetrachiral structures with long ligaments can be explained by observing the deformation of these systems. As one may observe from Figure 6(a), while in the case of on-axis loading, the square units rotate in opposite directions with respect to one another, which is the mechanism conducive for auxetic behaviour, when the same system is loaded in an off-axis direction, the deformation mechanism changes drastically (see Figurer 6(b)) and, instead, reverts to the
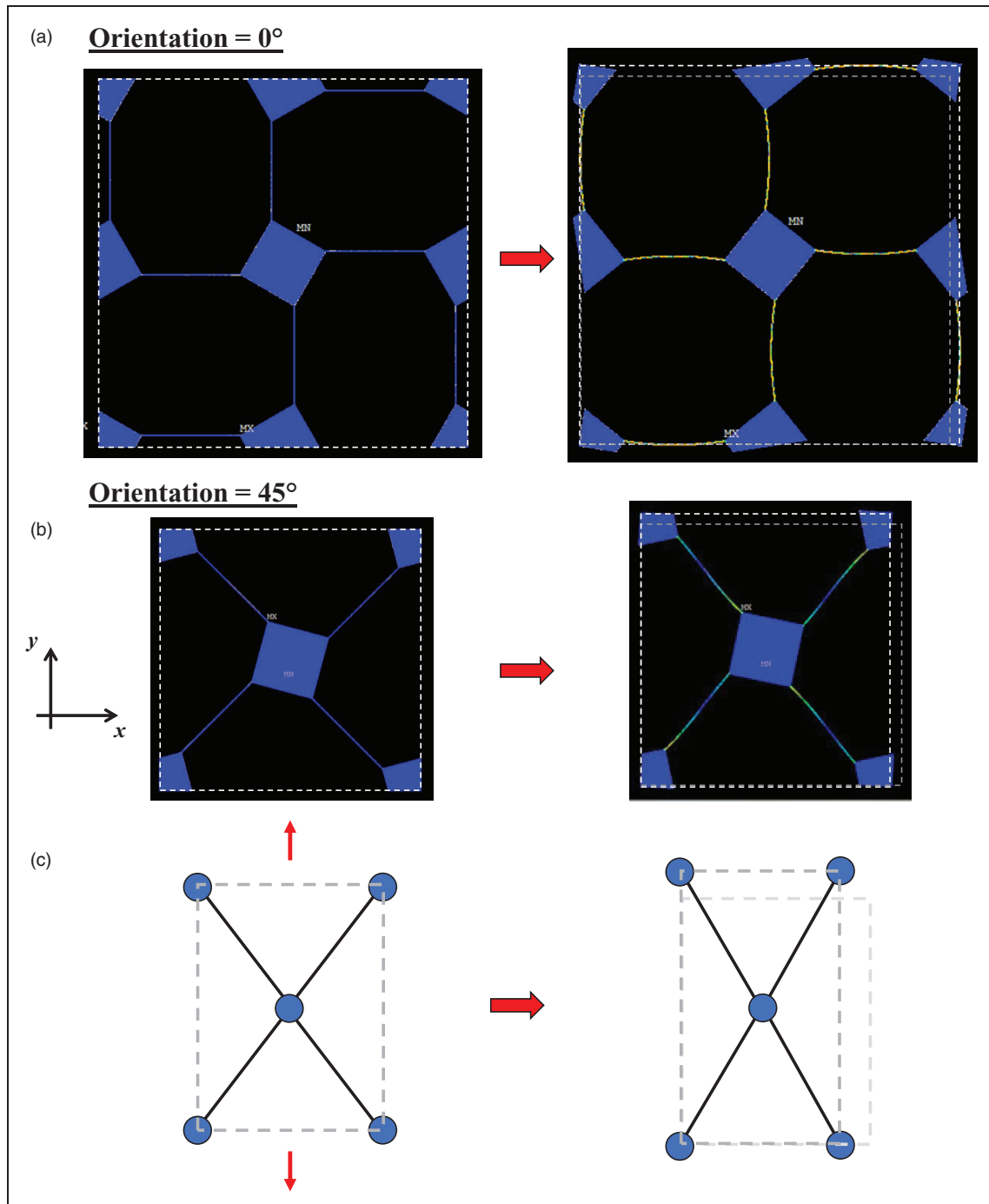
Figure 6. Diagrams showing the undeformed and deformed structures (with displacement scaling) for loading in the *y*-direction the simulated systems with the parameters: $l = 32$, $a = 20$, $w = 0.3$, $r = 0.1$ and $\theta = 30°$. The systems at (a) Orientation = 0° and (b) Orientation = 45° are shown. (c) A schematic of the so-called 'wine-rack' mechanism is also shown in order to highlight the similarity of this deformation mode with the deformation exhibited by the structure in (b).

'wine-rack' mechanism[56,57] (depicted in Figure 6(c)). This deformation mechanism, which has been studied extensively in relation to negative compressibility phenomena, is well-known to yield high positive Poisson's ratios. The change in deformation mode may be primarily attributed to the introduction of ligaments, since as observed in Figure 7, systems with no ligaments do not deform *via* this mechanism when loading in an off-axis direction and rotation of square units is still the predominant deformation

mode. Thus, the Poisson's ratio of this system remains relatively unchanged once the system is loaded in an off-axis direction.

The results obtained for the Young's moduli also highlight the large degree of anisotropy present in the systems with long ligaments. In Table 2, it is demonstrated that while for systems with $l = 0$ mm there is a drop of less than 5% in the Young's modulus of the structure once the system is loaded off-axis in comparison with its on-axis value, the systems with
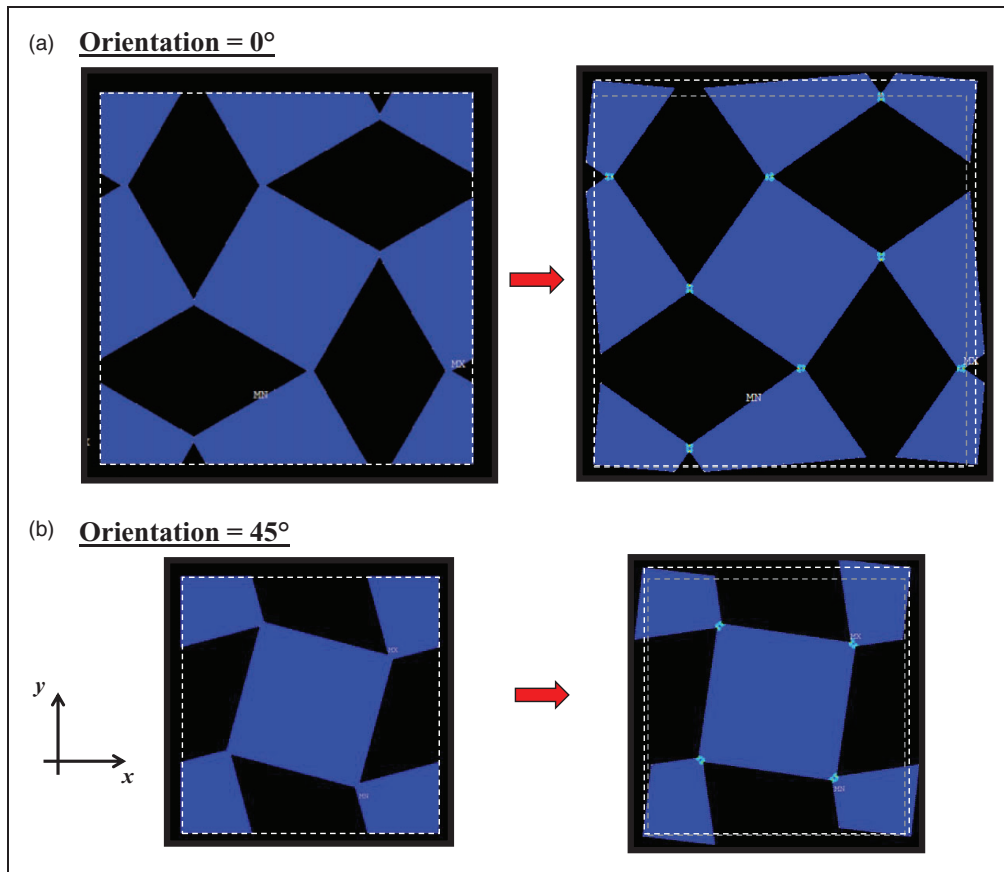
Figure 7. Diagrams showing the undeformed and deformed structures (with displacement scaling) for uniaxial loading in the *y*-direction the simulated systems with the parameters: $l = 0$, $a = 20$, $w = 0.3$, $r = 0.1$ and $\theta = 30°$. The systems at (a) Orientation $= 0°$ and (b) Orientation $= 45°$ are shown.

$l = 32$ mm show roughly a ten-fold decrease in stiffness. This effect can also be attributed to the change in deformation mechanism which alters the Poisson's ratio of the system. It is also worth noting that, as expected, the overall values for the Young's moduli of these systems decrease as the ligament length increases, with the structures with no ligaments showing the highest stiffness. This trend is characteristic of these systems and is congruent with findings from previous studies on similar structures.[43,49]

The findings for the shear moduli of these systems also indicate a number of intriguing trends. This property is not as commonly investigated as the Poisson's ratio and Young's modulus in mechanical metamaterials; however, it is also worth studying since certain auxetic systems such as auxetic foam have been shown to exhibit high shear resistance,[58,59] and therefore analysing this mechanical property could potentially reveal new advantageous characteristics. It is evident from Table 2 that the rotating square systems (i.e. the systems with $l = 0$) possess a relatively high shear modulus, which even exceeds the Young's modulus in magnitude. This indicates that this mechanism also has an extremely high resistance to shearing. This shear resistance is also exhibited for the ligamented systems, albeit at a much lower magnitude, since both the Young's and shear moduli of

these systems decrease drastically as ligament length increases. It is also interesting to note that while the system with $l = 0$ exhibits relatively little difference with respect to Young's modulus and Poisson's ratio when loaded in an on-axis and off-axis direction, the extent of anisotropy is far more pronounced in the case of the shear modulus. In fact, the shear modulus for these systems increases by roughly 2.5 times when the system is rotated by 45° from its on-axis orientation. The level of anisotropy increases in an exponential manner for the anti-tetrachiral systems as the ligament length increases, with the system possessing ligaments with length equal to 32 mm showing a 5-log difference between the shear modulus obtained for loading in an off-axis and on-axis direction.

These results highlight the significant influence which the addition of ligaments has on the mechanical properties and deformation mechanisms of these systems. Although the on-axis Poisson's ratio remains unchanged throughout, all other mechanical properties vary greatly for on-axis loading. Furthermore, the addition of ligaments and hence, the migration from a rotating square system to an anti-tetrachiral honeycomb, has an even greater influence on the off-axis properties, with the latter systems possessing a greatly more elevated level of anisotropy. In view of these

results, one may arrive at the conclusion that the ideal way to limit anisotropy and retain high stiffness is to employ the rotating squares mechanism for situations necessitating these requirements. However, this mechanism, as implemented in the current form for the basis of this study, suffers from one major drawback; it has inefficient stress distributions throughout the system, resulting in the formation of small regions of high concentrated stresses (namely the interconnection areas between square units), which could lead to the system yielding, and even fracturing, upon the application of very small strains. In order to counteract this problem, a recent study by Sorrentino et al.[55] explored how the interconnection regions may be geometrically optimized to improve stress distributions and increase the strain tolerance of the system. The resultant system (see Figure 4), produced using a double-radius filleting technique, results in a 'hybrid' system which shares a number of characteristics with both the rotating squares and anti-tetrachiral honeycombs; in that the system is made up predominantly of 'square' blocks of material which rotate and are connected together by 'joints' which may be characterised as extremely small ligaments. This geometric configuration has been demonstrated to exhibit greatly improved strain tolerance, whilst retaining a reasonably high level of effective stiffness. As mentioned previously, we have also examined the on-axis and off-axis responses of this system as well as those of the two corresponding rotating squares and anti-tetrachiral systems (see Figure 4(b)) through a run of simulations identical to that used for the first set of structures.

Optimized 'hybrid' structure and corresponding systems

The results for the analysis of the optimized structure and the two corresponding rotating square and anti-tetrachiral systems are presented in Table 3 and Figure 8.

It is evident from the values shown in Table 3 that the mechanical properties of the optimized geometry are more closely related to those of the equivalent anti-tetrachiral system than those of the rotating square system. However, there are still significant differences between these two systems. For example, the Young's moduli for both orientations of the 'hybrid' geometry are nearly double those of the anti-tetrachiral system, while the difference in the shear modulus is even more pronounced, especially for the $0°$ Orientation. As expected, the equivalent rotating square system is far stiffer than the other two geometries, however due to the relatively large thickness of the overlap region between square units, w, the large Young's and shear moduli are obtained at the cost of reduced auxeticity. In fact, while for Orientation $0°$, both the anti-chiral and 'hybrid' systems exhibit a Poisson's ratio of nearly -1, that of the rotating square system is -0.74.

The similarity of the deformations of the 'hybrid' geometry to both these corresponding structures may be observed in Figure 8, where the von Mises strain intensity factor, K_ε, contour plots are shown. This property was calculated as a ratio of the localized von Mises strain, $\varepsilon_{vonMises}$, to applied global strain, ε, as shown in equation (5).

$$K_\varepsilon = \frac{\varepsilon_{vonMises}}{\varepsilon} \tag{5}$$

In the case of uniaxial loading, ε is equal to the applied uniaxial strain ε_{ii}, while in the case of simple shear loading, it is defined by the applied global shear strain, ε_{ij}.

The K_ε factor is commonly used to quantitatively compare the localized strains found in different geometries upon loading independently of the intrinsic material properties and is particularly useful in this case since it does not depend on either the effective or material Young's moduli. It may also be used as a method to gauge the strain tolerance and fatigue limits of microstructures or machine components subjected to predetermined displacement loads under both static and dynamic conditions.[60,61] Systems with high K_ε values are more susceptible to material yielding and failure upon the application of a load than systems with lower values. In Figure 8, figures

Table 3. Results obtained for the 'hybrid' optimized geometry and its rotating square and anti-tetrachiral equivalents. Only one Poisson and Young's modulus value is presented per structure since the results were identical for loading in the x- and y-directions. The effective Young's moduli and shear moduli ratios (E* and G*) are calculated based on the material moduli ($E_{mat} = 200000$ MPa and $G_{mat} = 76923$ MPa). The parameter L represents the size of the orientation $= 0°$ unitcell.

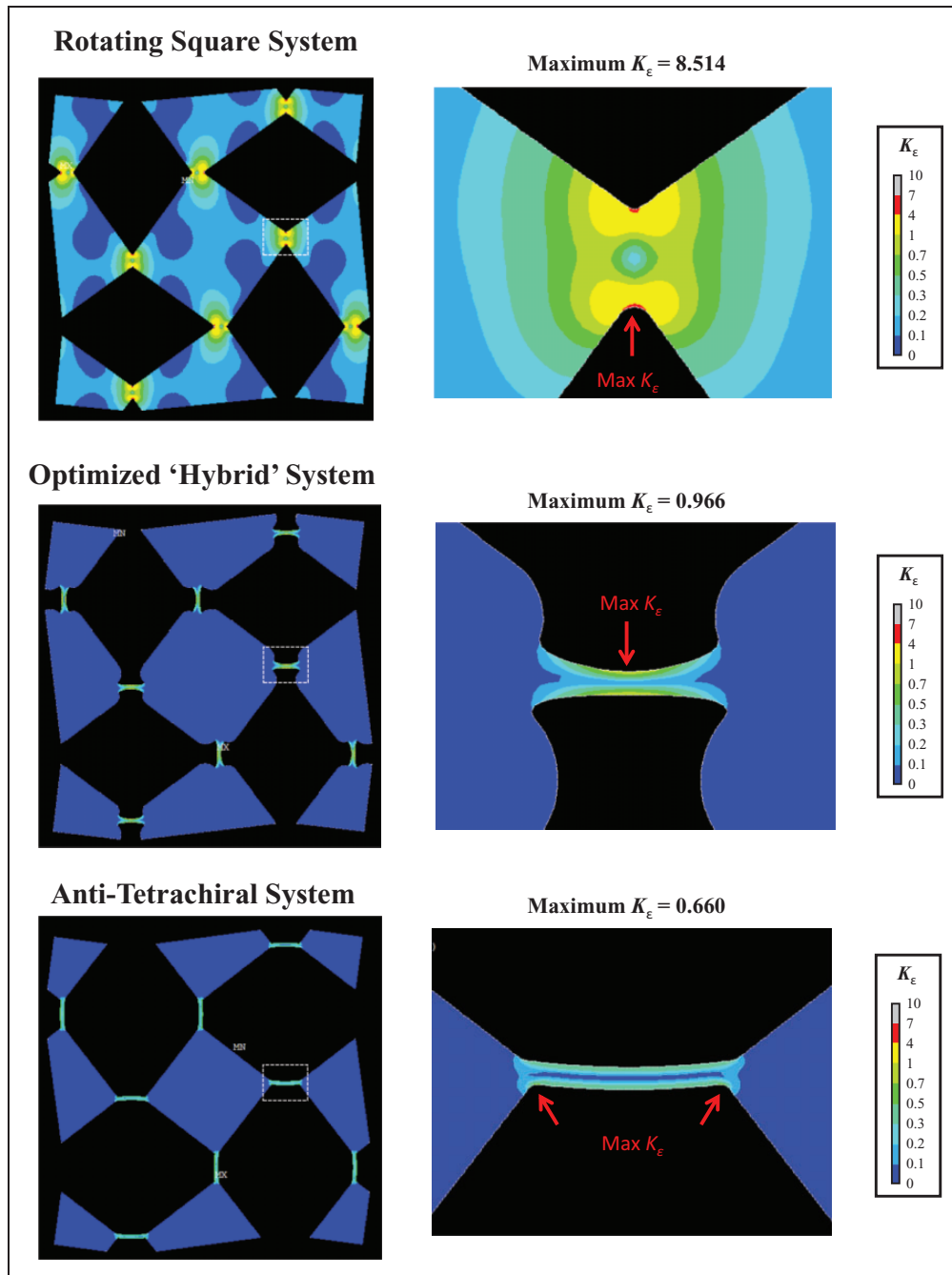| Geometry	L (mm)	ν	E (MPa)	G (MPa)	E^* (%)	G^* (%)
Orientation $= 0°$						
Rotating square	91.41	−0.743	10856	10001	5.43	13.00
Optimized 'hybrid'	91.39	−0.988	230	562	0.12	0.73
Anti-tetrachiral	90.75	−0.989	138	105	0.07	0.14
Orientation $= 45°$						
Rotating square	91.41	−0.525	9498	21128	4.75	27.47
Optimized 'hybrid'	91.39	−0.813	210	9418	0.11	12.24
Anti-tetrachiral	90.75	−0.503	104	6306	0.05	8.20

Figure 8. Diagrams showing the deformed structures at 3% uniaxial strain applied in the *y*-direction for Orientation $= 0°$. The strain intensity values, K_ε, were calculated based on the linear solutions and the deformations shown were obtained by magnified displacement scaling of the results obtained from the linearly solved simulation and are to be used mainly for the purpose of comparison between the deformation modes and interconnection region localized strain distributions of the three structures.

showing the K_ε distribution obtained for uniaxial loading of the Orientation $= 0°$ systems of these three structures are shown, while in Table 4 the maximum K_ε values obtained for each orientation and loading type (uniaxial and shear) of each structure are presented.

As shown in Figure 8, The maximum value obtained for the strain intensity factor of the 'hybrid' system is relatively low in comparison to that of the rotating square system (by nearly a factor of 10), and, in turn, slightly higher than that

of the anti-chiral structure. Furthermore, it is evident from Table 4 that this trend is also generally mirrored for shear loading conditions and for uniaxial loading in the 45° Orientation of these systems. In each case, the highest K_ε values are obtained for the rotating square system, while the anti-tetrachiral and 'hybrid' geometry show comparable values. The highest localized von Mises strains induced by deformation of the 'hybrid' system are also distributed throughout the interconnection region in a similar manner to that observed for the ligaments of the

Table 4. Results showing the maximum K_ε values obtained under linear uniaxial and shear loading conditions for the three systems at Orientation $= 0°$ and $45°$.

Geometry	Uniaxial loading	Shear loading
Orientation $= 0°$ Maximum K_ε		
Rotating square	8.514	2.541
Optimized 'hybrid'	0.966	1.009
Anti-tetrachiral	0.660	0.821
Orientation $= 45°$ Maximum k_ε		
Rotating square	6.710	4.199
Optimized 'hybrid'	0.908	2.197
Anti-tetrachiral	0.902	2.611

equivalent anti-tetrachiral system (see Figure 8). However, while in the latter the maximum localized strains are found at the ends of the ligament, in the 'hybrid' system it is found at the centre, similarly to the rotating square structure. This is most probably due to the non-uniform thickness of the interconnection 'ligament' in the 'hybrid' structure, which has the thinnest cross-section at the centre. This factor should also account for the higher stiffness of this geometric configuration in comparison with the anti-chiral system and its improved retention of auxeticity when loaded in the off-axis directions.

This last point is the main advantage of the 'hybrid' optimized structure over its anti-tetrachiral counterpart. In this structure, the lower maximum strain intensity factor and, hence improved deformability, of the 'hybrid' geometry over the rotating square system, does not come at a cost of greatly increased anisotropy as in the case of the anti-tetrchiral honeycomb. It is immediately evident, from Table 3, that once the 'hybrid' system is loaded at an Orientation of $45°$, a moderate reduction in the magnitude of the Poisson's ratio is observed, i.e. from -0.99 to -0.81. On the other hand, for the anti-tetrachiral system, the reduction is far more pronounced: from -0.99 to -0.50. This factor, along with the other findings of this study, indicates that through smart design and geometry optimization techniques similar to those employed in Sorrentino et al.,[55] it may be possible to design metamaterial structures which effectively capture, to a certain extent, the best features of two distinct classes of auxetic structures and combine them together. In the case study conducted here, we have shown that the 'hybrid' geometry has the ability to attain the high strain tolerance of the anti-tetrachiral honeycomb, whilst retaining the high level of isotropy found in the rotating square system. The findings of this work could also be potentially extended to the design of other 'hybrid' rotating structures such as those between rotating quadrilaterals and irregular anti-tetrachiral honeycombs, as well as rotating triangles and anti-trichirals (although it is well known that in the latter structure the introduction of ligaments

affects the Poisson's ratio in both on-axis and off-axis directions[19,62,63]) This work also highlights the importance of investigating the shear moduli and off-axis properties of auxetic systems since, as evidenced in this work, the effect of certain geometric alterations such as the introduction of ligaments can influence the deformation modes and mechanical properties of metamaterials in ways which cannot be observed and thoroughly studied from solely uniaxial on-axis loading analyses. Furthermore, future studies concerning the high-strain off-axis behaviour of these systems using nonlinear geometric and material properties, as well as experimental analyses, should also be carried in order to fully understand how the loading direction affects the mechanical properties and deformation behaviour of these auxetic systems.

Conclusions

In this work we have conducted a study to analyse the effect of the introduction of ligaments on the on-axis and off-axis properties of rotating unit auxetic metamaterials. We considered two different classes of auxetic systems, namely the rotating squares and anti-tetrachiral systems, which are geometrically very closely related to one another, and also compared the mechanical properties and deformation modes of these systems with those of an optimized 'hybrid' structure possessing geometric features related to both these metamaterials. The conclusions of this work may be summarized as follows:

- The rotating square system exhibits the highest level of structural stiffness and shear resistance, as well as the lowest level of anisotropy for off-axis loading. The system exhibits a high degree of auxeticity for both on-axis and off-axis uniaxial loading. On the other hand, the system suffers from severe localized strain/stress concentrations and an overall low global strain tolerance.
- The anti-tetrachiral system, which is essentially a 'ligamented' version of the rotating square system, shows a relatively reduced level of stiffness and a high extent of anisotropy which increases drastically with increasing ligament length. The system exhibits a large magnitude negative Poisson's ratio for on-axis loading, however the auxeticity of the system may be lost when loaded off-axis due to 'wine-rack'-like deformation modes induced by the presence of the ligaments. These disadvantages are partially offset by the high deformability and optimal distribution of localized stresses throughout the system.
- The 'hybrid' geometry possesses a stiffness level in the same logarithmic order of magnitude as the anti-tetrachiral system, albeit at a higher absolute value (double in the case studied here). It also has a localized stress/strain distribution profile which is

similar to the anti-tetrachiral geometry. However, it also exhibits a low level of anisotropy which is comparable to the rotating square system and thus retains its auxetic potential for loading both in an off-axis or an on-axis direction.

Declaration of Conflicting Interests

The author(s) declared no potential conflicts of interest with respect to the research, authorship, and/or publication of this article.

Funding

ORCID iDs

Andrea Spaggiari https://orcid.org/0000-0001-8959-2599
Davide Castagnetti https://orcid.org/0000-0003-3300-5716

References

1. Evans KE, Nkansah MA, Hutchinson IJ, et al. Molecular network design. *Nature* 1991; 353: 124–124.
2. Lakes R. Foam structures with a negative Poisson's ratio. *Science* 1987; 235: 1038–1040.
3. Alderson A. A triumph of lateral thought. *Chem Ind* 1999; 17: 384–391.
4. Fitzgerald A and Evans KE. The strain dependent indentation resilience of auxetic microporous polyethylene. *J Mater Sci* 2000; 5: 4039–4047.
5. Scarpa F, Giacomin JA, Bezazi A, et al. Dynamic behavior and damping capacity of auxetic foam pads. *Smart Mater Struct [Internet]* 2006; ■: 61690T. [AQ1]
6. Karathanasopoulos N, dos Reis F, Reda H, et al. Computing the effective bulk and normal to shear properties of common two-dimensional architectured materials. *Comput Mater Sci* 2018; 154: 284–294.
7. Tancogne-Dejean T, Karathanasopoulos N and Mohr D. Stiffness and strength of hexachiral Honeycomb-Like metamaterials. *J Appl Mech* 2019; 86: 111010.
8. Imbalzano G, Tran P, Ngo TD, et al. A numerical study of auxetic composite panels under blast loadings. *Compos Struct* 2016; 135: 339–352.
9. Tancogne-Dejean T and Mohr D. Elastically-isotropic elementary cubic lattices composed of tailored hollow beams. *Extrem Mech Lett* 2018; 22: 13–18.
10. Ali MN and Rehman IU. Auxetic polyurethane stents and stent-grafts for the palliative treatment of squamous cell carcinomas of the proximal and mid oesophagus: a novel fabrication route. *J Manuf Syst* 2014;. [AQ2]
11. Jacobs S, Coconnier C, Dimaio D, et al. Deployable auxetic shape memory alloy cellular antenna demonstrator: design, manufacturing and modal testing. *Smart Mater Struct* 2012; 21 [AQ3]
12. Huang S, Liu Y, Zhao Y, et al. Flexible electronics: stretchable electrodes and their future. *Adv Funct Mater* 2019; 29: 1805924–1805915.
13. Kolken HMA, Janbaz S, Leeflang SMA, et al. Rationally designed Meta-implants: a combination of auxetic and conventional meta-biomaterials. *Mater Horiz* 2018; 5: 28–35.
14. Masters IG and Evans KE. Models for the elastic deformation of honeycombs. *Compos Struct* 1996; 35: 403–422.
15. Gibson LJ, Ashby MF, Schajer GS, et al. The mechanics of two dimensional cellular materials. *Proc R Soc A Math Phys Eng Sci* 1782; 382: 25–42.
16. Grima JN, Gatt R, Alderson A, et al. On the potential of connected stars as auxetic systems. *Mol Simul* 2005; 13: 923–934.
17. Ai L and Gao XL. Micromechanical modeling of 3D printable interpenetrating phase composites with tailorable effective elastic properties including negative poisson's ratio. *J Micromech Mol Phys* 2017; 02: 1750015.
18. Grima JN and Evans KE. Auxetic behavior from rotating squares. *J Mater Sci Lett* 2000; 19: 1563–1565.
19. Grima JN and Evans KE. Auxetic behaviour from rotating triangles. *J Mater Sci* 2006; 41: 3193–3196.
20. ~~Grima JN, Manicaro E, Attard D, et al. Auxetic behaviour from connected different-sized squares and rectangles~~ Subject collections Auxetic behaviour from connected different-sized squares and rectangles. 2010; (August). [AQ4]
21. Wojciechowski KW. Two-dimensional isotropic system with a negative Poisson ratio. *Phys Lett A* 1989; 137: 60–64.
22. Prall D and Lakes RS. Properties of a chiral honeycomb with a poisson's ratio of -1. *Int J Mech Sci* 1997; 39: 305–314.
23. Alderson A, Alderson KL, Attard D, et al. Elastic constants of 3-, 4- and 6-connected chiral and anti-chiral honeycombs subject to uniaxial in-plane loading. *Compos Sci Technol* 2010; 70: 1042–1048.
24. Wu W, Hu W, Qian G, et al. Mechanical design and multifunctional applications of chiral mechanical metamaterials: a review. *Mater Des* 2019; 180: 107950.
25. Attard D, Farrugia PS, Gatt R, et al. Starchirals – a novel class of auxetic hierarchal structures. *Int J Mech Sci* 2020; 179: 105631.
26. Dudek KK. New type of rotation of chiral mechanical metamaterials. *Smart Mater Struct* 2020; 29: 115027.
27. Karathanasopoulos N, Reis F, Dos Diamantopoulou M, et al. Mechanics of beams made from chiral metamaterials: tuning deflections through normal-shear strain couplings. *Mater Des* 2020; 189: 108520.
28. Singamaneni S, Bertoldi K, Chang S, et al. Instabilities and pattern transformation in periodic. *Porous Elastoplastic Solid Coatings* 2009; 1: 1–6.
29. Yuan S, Chua CK and Zhou K. 3D-Printed mechanical metamaterials with high energy absorption. *Adv Mater Technol* 2019; 4: 1800419.
30. Silverberg JL, Evans AA, McLeod L, et al. Using origami design principles to fold reprogrammable mechanical metamaterials. *Science* 2014; 345: 647–650.
31. Sigmund O, Torquato S and Aksay IA. On the design of 1-3 piezocomposites using topology optimization. *J Mater Res* 1998; 13: 1038–1048.
32. Lim TC. Analogies across auxetic models based on deformation mechanism. *Phys Status Solidi Rrl* 2017; 11: 1600440.
33. Larsen UD, Signund O and Bouwsta S. Design and fabrication of compliant micromechanisms and

structures with negative Poisson's ratio. *J Microelectromech Syst* 1997; 6: 99–106.

34. Ishibashi Y and Iwata M. A microscopic model of a negative Poisson's ratio in some crystals. *J Phys Soc Jpn* 2000; 69: 2702–2703.

35. Mizzi L and Spaggiari A. Lightweight mechanical metamaterials designed using hierarchical truss elements. *Smart Mater Struct* 2020; 29: 105036.

36. Grima JN and Gatt R. Perforated sheets exhibiting negative Poisson's ratios. *Adv Eng Mater* 2010; 12: 460–464.

37. Bertoldi BK, Reis PM, Willshaw S, et al. Negative Poisson's ratio behavior induced by an elastic instability. *Adv Funct Mater* 2009; ■: 1–6. **[AQ5]**

38. Taylor M, Francesconi L, Gerendás M, et al. Low porosity metallic periodic structures with negative Poisson's ratio. 2013. **[AQ6]**

39. Mizzi L, Azzopardi KM, Attard D, et al. Auxetic metamaterials exhibiting giant negative Poisson's ratios. *Phys Status Solidi Rrl* 2015; 9: 425–430.

40. Mizzi L, Attard D, Evans KE, et al. Auxetic mechanical metamaterials with diamond and elliptically shaped perforations. *Acta Mech* 2021; 232: 779–791.

41. Slann A, White W, Scarpa F, et al. Cellular plates with auxetic rectangular perforations cellular plates with auxetic rectangular perforations. *Phys Status Solidi B* 2015; 252: 1533–1539.

42. Mizzi L, Salvati E, Spaggiari A, et al. 2D auxetic metamaterials with tuneable micro-/nanoscale apertures. *Appl Mater Today* 2020; 20: 100780.

43. Mizzi L, Grima JN, Gatt R, et al. Analysis of the deformation behavior and mechanical properties of Slit-Perforated auxetic metamaterials. *Phys Status Solidi* 2019; : 1800153. **[AQ7]**

44. Mizzi L, Gatt R and Grima JN. Non-porous grooved single-material auxetics. *Phys Status Solidi B* 2015; 252: 1559–1564.

45. Poźniak AA, Wojciechowski KW, Grima JN, et al. Planar auxeticity from elliptic inclusions. *Compos Part B Eng* 2016; 94: 379–388.

46. Yang W, Gao Z, Yue Z, et al. Hard-particle rotation enabled soft-hard integrated auxetic mechanical metamaterials. *Proc Math Phys Eng Sci* 2019; 475: 20190234.

47. Strek T, Jopek H, Maruszewski BT, et al. Computational analysis of sandwich-structured composites with an auxetic phase. *Phys Status Solidi B* 2014; 251: 354–366.

48. Strek T, Jopek H and Nienartowicz M. Dynamic response of sandwich panels with auxetic cores. *Phys Status Solidi B* 2015; 252: 1540–1550.

49. Gatt R, Attard D, Farrugia P-S, et al. A realistic generic model for anti-tetrachiral systems. *Phys Status Solidi B* 2013; 250: 2012–2019.

50. Gatt R, Brincat JP, Azzopardi KM, et al. On the effect of the mode of connection between the node and the ligaments in anti-tetrachiral systems. *Adv Eng Mater* 2015; 17: 189–198.

51. Grima JN, Alderson A and Evans KE. Negative Poisson's ratios from rotating rectangles. *Cmst* 2004; 10: 137–145.

52. Farrugia PS, Gatt R, Grima-Cornish JN, et al. Tuning the mechanical properties of the anti-tetrachiral system using nonuniform ligament thickness. *Phys Status Solidi B* 2020; 257: 1900507.

53. Dudek K, Wolak W, Gatt R, et al. Impact resistance of composite magnetic metamaterials. *Sci Rep* 2019; 9: 3963–3969.

54. Mizzi L, Attard D, Gatt R, et al. Implementation of periodic boundary conditions for loading of mechanical metamaterials and other complex geometric microstructures using finite element analysis. *Eng Comput* 2020; **[AQ8]**

55. Sorrentino A, Castagnetti D, Mizzi L, et al. Rotating squares auxetic metamaterials with improved strain tolerance. *Smart Mater Struct* 2021; 30: 035015.

56. Caruana-Gauci R, Degabriele E, Attard D, et al. Auxetic metamaterials inspired from wine-racks. *J Mater Sci* 2018; 53: 5079–5091.

57. Degabriele EP, Attard D, Grima-Cornish JN, et al. On the compressibility properties of the wine-rack-like carbon allotropes and related poly(phenylacetylene) systems. *Phys Status Solidi B* 2019; 256: 1800572.

58. Chan N and Evans KE. Fabrication methods for auxetic foams. *J Mater Sci* 1997; 32: 5945–5953.

59. Jin S, Korkolis YP and Li Y. Shear resistance of an auxetic chiral mechanical metamaterial. *Int J Solids Struct* 2019; 174-175: 28–37.

60. Ling B, Wei K, Wang Z, et al. Experimentally program large magnitude of Poisson's ratio in additively manufactured mechanical metamaterials. *Int J Mech Sci* 2020; 173: 105466.

61. Kamaya M. Low-cycle fatigue crack growth prediction by strain intensity factor. *Int J Fatigue* 2015; 72: 80–89.

62. Mizzi L, Mahdi EM, Titov K, et al. Mechanical metamaterials with star-shaped pores exhibiting negative and zero Poisson's ratio. *Mater Des* 2018; 146: 28–37.

63. Alderson A, Alderson KL, Chirima G, et al. The in-plane linear elastic constants and out-of-plane bending of 3-coordinated ligament and cylinder-ligament honeycombs. *Compos Sci Technol* 2010; 70: 1034–1041.